Bidirectional FtsZ filament treadmilling transforms lipid membranes via torsional stress

Diego Ramirez-Diaz
Max Planck Institute of Biochemistry
Adrian Merino-Salomon
Max Planck Institute of Biochemistry
Fabian Meyer
Kiel University
Michael Heymann
University Stuttgart https://orcid.org/0000-0002-9278-8207
German Rivas
Centro de Investigaciones Biológicas
Marc Bramkamp
Kiel University
Petra Schwille (schwille@biochem.mpg.de)
Max Planck Institute of Biochemistry https://orcid.org/0000-0002-6106-4847

Article

Keywords: Bacterial Cell Division, Self-organization, Shape Deformation, Soft Lipid Tubes, Optical Tweezers, Membrane Budding

Posted Date: November 9th, 2020

DOI: https://doi.org/10.21203/rs.3.rs-91093/v1

Version of Record: A version of this preprint was published at Nature Communications on June 3rd, 2021.
See the published version at https://doi.org/10.1038/s41467-021-23387-3.

Abstract

FtsZ is a key component in bacterial cell division, being the primary protein of the presumably contractile Z ring. *In vivo* and *in vitro*, it shows two distinctive features that could so far however not be mechanistically linked: self-organization into directionally treadmilling vortices on solid supported membranes, and shape deformation of flexible liposomes. In cells, circumferential treadmilling of FtsZ was shown to recruit septum-building enzymes, but an active force production remains elusive. To gain mechanistic understanding of FtsZ dependent membrane deformations and constriction, we designed an *in vitro* assay based on soft lipid tubes pulled from FtsZ decorated giant lipid vesicles (GUVs) by optical tweezers. FtsZ actively transformed these tubes into spring-like structures, where GTPase activity promoted spring compression. Operating the optical tweezers in lateral vibration mode and assigning spring constants to FtsZ coated tubes, the directional forces that FtsZ-YFP-mts rings exert upon GTP hydrolysis can be estimated to be in the pN range. They are further shown to induce membrane budding with constricting necks on both, giant vesicles and *E.coli* cells devoid of their cell walls. We hypothesize that these forces are generated by bidirectional treadmilling through torsional stress.

Main Text

In biology, fundamental mechanical processes, such as cell division, require an intricate space-time coordination of respective functional elements. However, how these elements, mostly proteins, can self-organize to exert forces driving large-scale transformations is poorly understood. In several organisms, ring-like cytoskeletal elements appear upon cytokinesis; for instance, the FtsZ-based contractile Z ring in bacteria. Ring-like FtsZ structures have previously been shown to deform liposome membranes (1,2). When reconstituted on flat membranes, FtsZ self-assembles into rotating-treadmilling vortices with conserved direction (3,4). *In vivo*, FtsZ shows circumferential but bidirectional treadmilling that is assumed to serve as a pacemaker guiding peptidoglycan synthesis around the septum (5,6).

Despite of these exciting findings, it is not clear whether these treadmilling FtsZ filaments actively contribute to the physical process of lipid membrane constriction and cytokinesis in bacteria (7,8). The challenge is two-fold: (i) to determine the forces that are actually required to divide a bacterial cell with its much more complex architecture than a membrane shell, and (ii) to formulate the exact mechanism by which forces on membranes could at all be exerted by FtsZ treadmilling filaments. For instance, considering the mechanical bearing related to internal turgor pressure (~MPa), models have suggested that FtsZ forces in the range of 8-80 pN would be required for constriction (9). In contrast, it has been proposed that turgor pressure need not be considered, due to the possibility of same osmolarity between periplasm and cytoplasm (10). For this case, very low FtsZ forces in the range of 0.35 – 2.45 pN could exert membrane deformations leading to constriction (10). In conclusion, *in vivo* and *in vitro* experimental approaches addressing those two major questions are needed to gain deeper understanding in cell division in bacteria. While (i) can only be addressed by extensive *in vivo* studies and may remain a

notorious challenge in bacterial cell biology for many years, (ii) is more readily accessible by state-of-the-art biophysics on *in vitro* reconstituted systems, aiming at elucidating the mechanistic features of FtsZ as a membrane deforming polymer.

Thus, regardless of whether or not FtsZ is the major force contributor in cell division, it remains a fundamental question whether the energy-dissipating treadmilling phenomenon can be assigned a force-inducing role at all, and if so, how this force could be transmitted to constrict the membrane. We here introduce a new experimental strategy to produce cylindrical membrane geometries mimicking rod-like bacterial shapes, by pulling soft lipid tubes from deflated giant unilamellar vesicles (GUVs) using optical tweezers. Our aim is to quantitatively elucidate the physical principles underlying membrane deformations induced by dynamic FtsZ rings and the scale of delivered forces. These particular principles are key to understand the nature of FtsZ membrane deformations *in vitro* and *in vivo*.

Based on our recent study (3), we externally added FtsZ-YFP-mts to GUVs made of *E. coli* lipid extract. Conditions to obtain ring-like structures were determined by tuning GTP and Mg^{+2} (Fig. 1A). Since no clear deformations were observed for tensed vesicles (Fig. 1A), we designed a two-side open chamber allowing for slow water evaporation to obtain deflated and deformable GUVs. After 20-30 minutes, we evidenced that rings were inducing inwards-cone structures emerging from the membrane surface, indicative of drilling-like inward forces (Fig. 1B). Motivated by this specific geometry, we designed PDMS microstructures mimicking such inward cones (Fig. 1C Fig 1SA). After coating these with supported lipid bilayer (SLB) and triggering protein polymerization, we observed individual filaments/bundles to wrap the cone in a dynamic fashion resembling a vortex (Fig. 1D) (Movie S1). We noticed that the dynamic vortices rotate both clockwise and anticlockwise (Fig. 1E), indicating that preferential directionality observed on flat SLBs is absent in conical geometry. Rotational velocities were estimated around showing relatively good agreement with our previous results on flat surfaces () (3).

To quantitatively characterize the impact of FtsZ on soft tubular geometries, we developed a method based on optical tweezers. Contrary to prior approaches using micropipettes (11), we pulled soft tubules from weakly surface-attached GUVs (Fig. 2A) by moving the GUVs relative to an optically trapped bead. Lipid tubes with mean diameter of ca. (Fig. 2SA) were now pulled from deflated GUVs decorated with ring-like FtsZ structures and inward-conical deformations (Movie S2). Given the mobility of FtsZ rings and filaments over the GUV surface, protein from the vesicle started entering the tube immediately after pulling. After 175s, helical tube shapes were clearly observed (Fig. 2B), indicative of dynamic coiling (Movie S3). As more protein entered the tube, the spring-like structure became compressed (Fig. 2B, 500s). These helical tube deformations can be rationalized by twisting of an elastic rod subjected to constant tensile force (Fig. 3F). Similar to the experiment in Fig. 1D, filaments grew towards (clockwise)

and away from (counterclockwise) the tip of the tube. If filament growth imposes torsion, the counter-growing filament will generate torsion in the opposite direction. The importance of the bidirectional treadmilling, or bidirectional filament growth, can be understood using a shoelace analogy: opposite torque should be exerted on both ends of the shoelace to observe a helical deformation. If one end is loose, the opposite end will only rotate accordingly (sliding).

Since spring-like deformations were observed with a FtsZ protein chimera that binds autonomously to membrane (FtsZ-YFP-mts), we attempted to confirm whether this phenomenology is intrinsic to the FtsZ polymer and not due to chimera artifacts, e.g. induced by the membrane targeting sequence. Based on the reconstitution of dynamic rings on flat membranes using the *E.coli* FtsZ natural anchor ZipA (12), we aimed to establish appropriate conditions for WT-FtsZ rings externally decorating GUVs using ZipA. First, as a control, ZipA-decorated vesicles were examined under deflation conditions, and none of them showed inwards deformations (N=14, Fig. 2SB). In addition, we pulled lipid tubes with only ZipA and none showed any relevant deformation over time (N=10, Fig. 2SB). Only after adding wild type FtsZ, we obtained rings and inward deformations (Fig. 2B). We then pulled tubes from these vesicles and observed helical transformations (Fig. 2C) (N=3 out of 18 pulled tubes), indicating that FtsZ polymer and not its membrane attachment (in this case ZipA) caused this effect. Interestingly, FtsZ+ZipA (as well as FtsZ-YFP-mts) displayed in plectonic/supercoiled regions (Fig. 2C, Fig. 1SE) as further indicative of torsion over the lipid tube.

After having established that the spring-like membrane transformations do not result from membrane anchors only, we needed to distinguish the active role of GTP-dependent FtsZ treadmilling. To investigate the role of GTP hydrolysis for the spring-like deformations, we reconstituted FtsZ-YFP-mts*[T108A], a mutant with low GTPase activity (3). FtsZ-YFP-mts*[T108A] also self-assembles into ring-like structures (Fig. 1SB) with similar polymerization rates as compared to FtsZ-YFP-mts, but lacks dynamic treadmilling. Reconstituted on soft vesicles, FtsZ-YFP-mts*[T108A] rings (Fig. 1SB) also induce cone-like deformations (Fig. 1SC) as well as helical deformations, after 300 s, in lipid tubes (Fig. 3B). The pitch of these helices however remained unaffected () at longer times (900s, Movie S4). In contrast, helices decorated with GTP-active FtsZ-YFP-mts (Fig. 3A) underwent compression to a pitch of already before 300s. By plotting the arc-length of the spring against FtsZ density on the tubes in Fig. 3A&B as a function of time (Fig. 2SD), we clearly observed a greater membrane-deforming activity for FtsZ-YFP-mts (Fig. 3C). The time-scale of deformations likely depends of the amount of protein on the tube. Thus, since the initial amount of protein on the tubes varies among independent experiments, further statistical analysis was performed in steady state.

Since the deflation of individual GUVs could fluctuate, we also tested whether compression could be biased by GUV membrane tension and protein density over the tube. The tube diameter represented our observable for membrane tension according to the relation , where denotes the lipid bending modulus and the membrane tension (11,13). The lower the membrane tension by deflation, the larger the tube diameter. Therefore, we plotted the mean pitch vs tube diameter (Fig. 3D), considering also the amount of protein (Fig. 3D-insert). Although there was a mild correlation between pitch and diameter (Fig. 3D) for FtsZ-YFP-mts (N=12), the mean pitch was consistently longer for (N=10) FtsZ-YFP-mts*[T108A] (Fig. 3D) in the case of tubes with comparable or higher protein density (Fig. 3C-insert). To better visualize the impact of GTPase activity, we plotted the pitch distribution for both proteins: the GTPase activity contributed to a decrease of pitch (Fig. 3E) as clear indicative of spring compression. Interestingly, both distributions can be reasonably considered to be bimodal. We suggest this might indicate two states of torsion: a structural intrinsic torsion (longer pitch) that is further enhanced (shorter pitch) via GTPase activity (Fig. 3F). Note that FtsZ-YFP-mts*[T108A] exhibits residual GTPase activity, driving some compression and potentially explaining the bimodality of this distribution.

To assess mechanical properties of FtsZ-YFP-mts-induced spring-like structures, we implemented an alternative approach based on the elastic response of the GUV+tube system to a specific dynamic input. Using a piezoelectric stage, we induced a lateral oscillation of the GUV position () and recorded forces by the optical trap (Movie S5). We here measured the resistive force of the material per micrometer (k-spring constant). The stiffer the material, the higher force detected by the optical trap. To calculate the amplitude of the signal at 1 Hz, the signal was Fast Fourier Transformed, as depicted in Figure 4B, where the magenta line refers to the pure lipid tube and the green line to FtsZ. The pure lipid contribution (N=11) yielded values between 0.15 – 0.55 pN/ (Fig. 4D), while values between 0.23 – 1.52 pN/ (Fig. 4D) were obtained for FtsZ. Although forces were recorded for tubes fully covered with FtsZ (Fig. 4A); for some vesicles, the lipid response still dominated the spring constant measurement, meaning that some FtsZ data points lie between 0.15 – 0.55 pN/ (dashed magenta lines, Fig. 4D). Thus, FtsZ data points overlapping the lipid contribution were discarded for further analysis, since they likely did not contribute to the FtsZ force signal (Fig. 4D-insert). Interestingly, in our GUVs *in vitro* assays (also encapsulated rings, see Fig. 5D), we observed that discernible FtsZ-YFP-mts rings appeared to be of fairly similar size and brightness (Fig 2SE, with N=412 analyzed rings). To estimate the range of forces that these ring units could exert in our particular assays, we took advantage of the fact that some ring-decorated vesicles flattened on the glass surface (Fig. 4B) allowing precise imaging of single rings on the surface using the same conditions as in the FtsZ coated tubes. Although the absolute number of monomers or filaments comprising these treadmilling ring units is unknown, we can assign the measured forces of around 1 pN driving the transformation of a lipid tube into a helical structure to these discernible FtsZ-YFP-mts ring units. This coarse estimation did not exclude any possible intrinsic lipid contribution.

Interestingly, we had previously inferred that FtsZ-YFP-mts rings on SLB are made of filamentous structures of 0. length in average (3). This estimation could be used to validate our force measurements. Assuming a persistence length as , FtsZ filaments would exhibit a flexural rigidity that agrees well with previous experimental reports (14). Based on this, we could assess the Young's modulus of FtsZ filaments: (where , the area moment of inertia, nm (15)). On the other hand, the Young's modulus of a spring is related to the spring constant through , where denotes the spring constant, is the spring initial length and the cross-section. By considering two independent hollow cylinders, one made of lipid bilayers (lipid bilayer thickness: ~5 nm) and one made of FtsZ-YFP-mts (one FtsZ monomer diameter: ~5 nm), the ratio was fairly constant in our tube experiments, and therefore the relationship is reasonably valid. To calculate , we here considered raw averages for distributions shown in Fig. 4D and subtracted the lipid contribution in the case of FtsZ: pN/ and pN/. Then, the ratio showed good agreement compared to assuming (lipids with bending . This confirmed that our force measurements corresponded well with previous flexural rigidity values for FtsZ fibers. In addition, our data provide further evidence that FtsZ filaments are softer than other cytoskeleton proteins such as microtubules () or actin () (18,19)

The helical nature of FtsZ and its torsional dynamics have been experimentally observed (20, 21); however, its relation to a potential mechanism of actively deforming membranes has not yet been clearly established. According to our observations, the helical membrane transformation caused in this study by FtsZ filaments can best be understood by assuming Darboux torque around the lipid tube. Darboux torques are tangential torques caused by a local mismatch between the plane defined by the filament curvature and the membrane attachment direction (22). This twisting angle along the one filament is key to produce torque. A molecular dynamics study showed that dynamin, a helical endocytic constriction protein, required twisting of the "adhesive-stripe" to achieve full membrane hemifusion (22). In the case of FtsZ, molecular dynamics studies have predicted an angle of "twisting" along the c-terminus, where membrane attachment occurs (23, 24). Also, Fierling and coworkers have theoretically studied membrane deformations produced by filaments inducing torques (25). Strikingly, they found inward vortex-like deformations from flat surfaces and spring-like shapes when filaments wrapped around a tubular geometry (25). These predictions agree remarkably well with our observations.

So far, we had investigated an inverse geometry, i.e., FtsZ added from the outside, as compared to the physiological case. Now, we also reconstituted FtsZ-YFP-mts and FtsZ-YFP-mts*[T108A] inside GUVs (Fig. 5A). Conditions to obtain ring-like-structures (Fig. 5B) or filaments wrapping the vesicle (Fig. 1SD) were again found by tuning GTP and Mg^{+2}. Interestingly, the diameters of FtsZ-YFP-mts*[T108A] rings were significantly larger () than FtsZ-YFP-mts () (Fig. 5D). This difference was not observed in the case of SLBs (3), suggesting that the deformability of the lipid surface affects the steady state of FtsZ assembly. In other words, the physical properties of the membrane may play an important role in FtsZ fragmentation and treadmilling. In addition, the wide size distribution in the low GTPase mutant case

(Fig. 5D) might indicate that polymers were more flexible to accommodate a larger variety of curvatures. Strikingly, both FtsZ mutants could create outwards deformations emerging from rings (Fig. 5E). But only in the case of FtsZ-YFP-mts, there was clear evidence of ring constriction (Fig. 5E) similar to previous reports (1). Based on Fig. 1 and our previous findings (3), we hypothesize that FtsZ ring formation could create outwards out-of-plane forces due to filament structure and polarity (Fig. 5F). However, inactive FtsZ filaments only exhibiting static (structural) torsion are unable to stabilize smaller diameters. In contrast, dynamic treadmilling upon GTP-hydrolysis drives constriction and condensation (Fig. 5G), such that active FtsZ filaments lead to an overall shrinkage of diameters. Indeed, 80% (N=21/26) vesicles showed outwards deformations and constriction necks simultaneously; in contrast to 26% for FtsZ-YFP-mts*[T108A]. FtsZ constriction and neck formation (from inside) thus represents an analog of helix compression when the protein wraps the lipid tube (from outside).

Although it has been pointed out that these mechanistic studies on FtsZ in controlled membrane environments may not easily be transferred to the situation *in vivo*, it is tempting to evaluate the ability of FtsZ-YFP-mts construct to deform and actuate lipid membranes in a more physiological setting. Therefore, *E. coli* cells were transformed with a plasmid containing the corresponding gene under control of an inducible promoter. Upon IPTG induction, FtsZ-YFP-mts fluorescence signals in the cells were observed. The FtsZ-YFP-mts construct localizes in several ring-like structures around midcell (Fig. 6A). Multiple Z-ring structures were observed, due to the overexpression of the FtsZ-YFP-mts protein. A 3D-reconstruction reveals that these FtsZ assemblies are indeed ring structures that resemble those formed by native FtsZ rings at the division site (Fig. 6B). Importantly, without addition of inductor, no FtsZ-YFP-mts structures were observed (Fig. 6A). Since FtsZ driven membrane deformations could not be observed in tensed GUVs (Fig. 5), we reasoned that they were even less likely to appear in walled bacteria with turgor pressure. Therefore, cells were treated with lysozyme to create *E. coli* spheroplasts in osmoprotective media. Cells expressing the FtsZ fusion protein were highly fragile and prone to lysis. We therefore started microscopic analyses before all cells have converted to spheroplasts (Fig. 6A). Importantly, vesicular structures budding out from spheroplasted cells were observed (Fig. 6A, arrows). These vesicular structures were not observed in control cells lacking the FtsZ-YFP-mts expression, indicating that they are a consequence of protein overproduction. However, in the MBL medium, the occurrence of FtsZ-YFP-mts budding was low (Fig. 6A). In contrast, similar lysozyme treatment in sucrose-buffer showed cells with i) small outwards deformations (irregular surface) that correlate with a regions higher protein density and ii) swelled cells with clear vesiculation (Fig. 6C, Movie S6). A membrane stain confirmed that areas with strong FtsZ fusion protein assemblies displayed lipid membrane budding (Fig. 3S) and constriction necks. Although the presence of cells with irregular surfaces (small outwards deformations), single and multiple vesiculation was not exclusive of over-expression, the frequency of such events clearly increased due to FtsZ-YFP-mts (Fig. 6D). Further interesting phenotypes such as cells connected by lipid tubes or “pearl-necklaces” were observed (Fig. 3S). These results agreed remarkably well with our outwards deformations and constriction necks from FtsZ rings inside GUVs. Directional screw-like forces promoting extrusion of lipid material or budding (Fig.

5H & Fig. 6B), as well as constriction necks (Fig. 5G & Fig. 6C), are both explained in terms of a FtsZ polymer able to exert torsional stress as explained above. Interestingly, this demonstrates the possibility of FtsZ filaments playing an active role in cell division organisms that divide by budding, such as *Acholeplasma laidlawii* (28).

Altogether, our experiments provide clear evidence that FtsZ induces two kinds of mechanical deformations to membranes. First, static (structural) FtsZ torsion by the self-assembly of curved polar filaments into rings on flat surfaces that induces inwards/outwards deformations as described earlier (3). Second, an additional dynamic torque-twist induced by circumferential treadmilling powered by GTP hydrolysis, stabilizing smaller ring diameters and supporting further membrane constriction. Regardless whether protein was externally added or encapsulated, cylindrical geometry allowed clockwise and anti-clockwise treadmilling (Fig. 5G). Together, active FtsZ induces helical transformation of the membrane tube and a super-constricted state of filaments, imposing a mechanical strain that promotes breakage and therefore the emergence of treadmilling (Fig. 5F). This establishes an interesting similarity between FtsZ and dynamin, in which GTP hydrolysis also triggers a super-constricted state, favoring fragmentation and clustering (19,20). For the case of FtsZ-YFP-mts, we conclude that these torques represent a robust constriction mechanism for flat and cylindrically shaped membranes, generating forces in the pN range. These FtsZ-induced forces drive outwards deformations and constriction necks in the case of deflated vesicles *in vitro* and wall-less *E. coli in vivo*.

Although the here reported forces range do not likely suffice for the entire process of bacterial cytokinesis of walled rod-like cells, given the temporal relevance of FtsZ dynamics in the coordination of synthesis of new wall material (5,6), an initial inwards membrane deformation may be key to trigger cytokinesis in the form of a “FtsZ curvature trigger”. Interestingly, viable FtsZ-GTPase mutants (6) as well as temperature-sensitive mutants (29) exhibit abnormal septum formation or “twisted” septum. In agreement with our data, GTPase FtsZ deficient mutants could generate inwards membrane deformations along a helical FtsZ filament. Due to the lack of further twisting/condensation in FtsZ, the synthesis of new wall material would follow a relaxed-helix pattern (twisted septum) rather than a compressed-helix or “ring” Regardless of GTPase activity, we also hypothesize that if the membrane tension is lowered by incorporation of de novo synthesized lipids in the division site (10), the here reported forces range might become relevant for the initiation of cell division.

References

1. T Osawa, D. E. Anderson, H. P. Erickson, Reconstitution of Contractile FtsZ Rings in Liposomes. *Science*. **320**, 792–794 (2008).

2. Osawa, H. P. Erickson, Liposome division by a simple bacterial division machinery. *PNAS*. **110**, 11000–11004 (2013).
3. A. Ramirez-Diaz *et al.*, Treadmilling analysis reveals new insights into dynamic FtsZ ring architecture. *PLOS Biology*. **16**, e2004845 (2018).
4. Loose, T. J. Mitchison, The bacterial cell division proteins FtsA and FtsZ self-organize into dynamic cytoskeletal patterns. *Nat Cell Biol*. **16**, 38–46 (2014).
5. W. Bisson-Filho *et al.*, Treadmilling by FtsZ filaments drives peptidoglycan synthesis and bacterial cell division. *Science*. **355**, 739–743 (2017).
6. Yang *et al.*, GTPase activity–coupled treadmilling of the bacterial tubulin FtsZ organizes septal cell wall synthesis. *Science*. **355**, 744–747 (2017).
7. Holden, S. Probing the mechanistic principles of bacterial cell division with super-resolution microscopy. *Current Opinion in Microbiology*. **43**, 84–91 (2018).
8. Coltharp, C. & Xiao, J. Beyond force generation: Why is a dynamic ring of FtsZ polymers essential for bacterial cytokinesis? **39**, e201600179 (2017).
9. Lan, G., Wolgemuth, C. W. & Sun, S. X. Z-ring force and cell shape during division in rod-like bacteria. **104**, 16110–16115 (2007).
10. Osawa, M. & Erickson, H. P. Turgor Pressure and Possible Constriction Mechanisms in Bacterial Division. *Microbiol.* **9**, (2018).
11. Roux *et al.*, Membrane curvature controls dynamin polymerization. *PNAS*. **107**, 4141–4146 (2010).
12. Krupka, M., Sobrinos-Sanguino, M., Jiménez, M., Rivas, G. & Margolin, W. Escherichia coli ZipA Organizes FtsZ Polymers into Dynamic Ring-Like Protofilament Structures. **9,** (2018).
13. Bassereau, P., Sorre, B. & Lévy, A. Bending lipid membranes: Experiments after W. Helfrich's model. *Advances in Colloid and Interface Science*. **208**, 47–57 (2014).
14. J. Turner *et al.*, The Mechanics of FtsZ Fibers. *Biophysical Journal*. **102**, 731–738 (2012).
15. Huecas, S. *et al.* Energetics and Geometry of FtsZ Polymers: Nucleated Self-Assembly of Single Protofilaments. *Biophysical Journal.* **94**, 1796–1806 (2008).
16. Picas, F. Rico, S. Scheuring, Direct Measurement of the Mechanical Properties of Lipid Phases in Supported Bilayers. *Biophysical Journal*. **102**, L01–L03 (2012).
17. Rawicz, W., Olbrich, K. C., McIntosh, T., Needham, D. & Evans, E. Effect of Chain Length and Unsaturation on Elasticity of Lipid Bilayers. *Biophysical Journal* **79**, 328–339 (2000).
18. Gittes, B. Mickey, J. Nettleton, J. Howard, Flexural rigidity of microtubules and actin filaments measured from thermal fluctuations in shape. *The Journal of Cell Biology*. **120**, 923–934 (1993).
19. van Mameren, K. C. Vermeulen, F. Gittes, C. F. Schmidt, Leveraging Single Protein Polymers To Measure Flexural Rigidity. *J. Phys. Chem. B*. **113**, 3837–3844 (2009).
20. Szwedziak, Q. Wang, T. A. M. Bharat, M. Tsim, J. Löwe, Architecture of the ring formed by the tubulin homologue FtsZ in bacterial cell division. *eLife*. **3**, e04601 (2015).

21. Arumugam, S. *et al.* Surface Topology Engineering of Membranes for the Mechanical Investigation of the Tubulin Homologue FtsZ. *Angewandte Chemie International Edition* **51**, 11858–11862 (2012).
22. Pannuzzo, Z. A. McDargh, M. Deserno, The role of scaffold reshaping and disassembly in dynamin driven membrane fission. *eLife*. **7**, e39441 (2018).
23. G. de P. Salas *et al.*, Torsion and curvature of FtsZ filaments. *Soft Matter*. **10**, 1977–1986 (2014).
24. Hsin, A. Gopinathan, K. C. Huang, Nucleotide-dependent conformations of FtsZ dimersand force generation observed through molecular dynamics simulations. *PNAS*. **109**, 9432–9437 (2012).
25. Fierling, A. Johner, I. M. Kulić, H. Mohrbach, M. M. Müller, How bio-filaments twist membranes. *Soft Matter*. **12**, 5747–5757 (2016).
26. Colom, L. Redondo-Morata, N. Chiaruttini, A. Roux, S. Scheuring, Dynamic remodeling of the dynamin helix during membrane constriction. *PNAS*. **114**, 5449–5454 (2017).
27. Takeda *et al.*, Dynamic clustering of dynamin-amphiphysin helices regulates membrane constriction and fission coupled with GTP hydrolysis. *eLife*. **7**, e30246 (2018).
28. Gao, Y. (2019). Cell division in walled Bacillus subtilis and cell wall-lacking Acholeplasma laidlawii. PhD thesis, University of Amsterdam.
29. Addinall, S. G. & Lutkenhaus, J. FtsZ-spirals and -arcs determine the shape of the invaginating septa in some mutants of Escherichia coli. *Microbiol.* **22**, 231–237 (1996).

Declarations

Acknowledgments: We acknowledge Sven Vogel, Allen Liu and Ethan Garner and for very useful discussions. We thank Daniela Garcia, Ana Raso and the MPIB Core Facility for assistance in FtsZ-YFP-mts protein purification. This work was funded through MaxSynBio (MPG together with Federal Ministry of Education and Research of Germany) grant number 031A359A to PS, and the Transregio CRC 174 by the DFG (Deutsche Forschungsgemeinschaft) to PS and MB. Work at GR lab was supported by Spanish Government Grants BFU2016-75471-C2-1-P and 2019AEP088. The authors have declared that no competing interests exist. All data is available in the main text or the supplementary materials.

Code availability

All custom code is available on request.

Data availability

All data are available in the main text, the supplementary materials, or upon request.

Figures

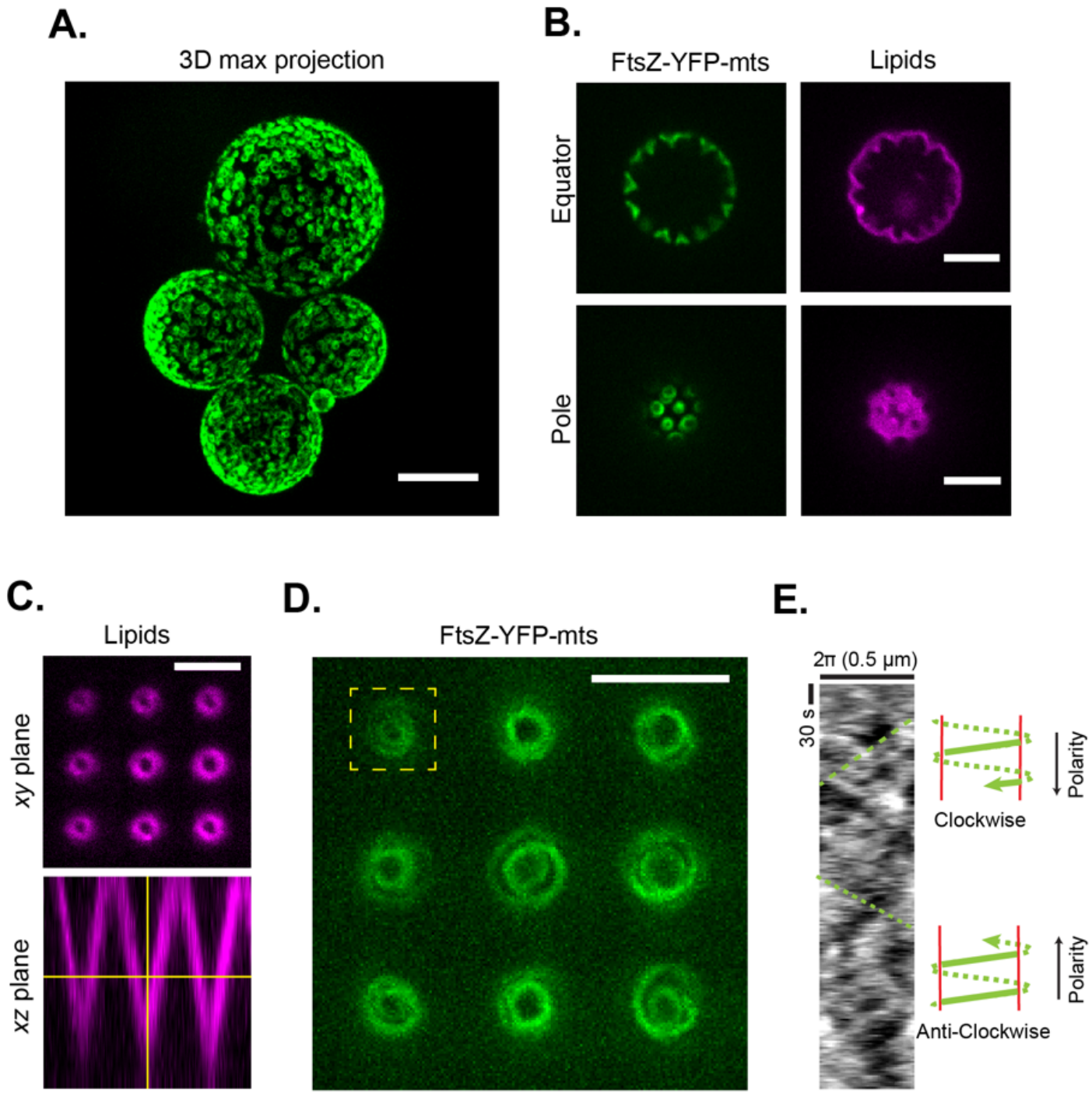

Figure 1

A) FtsZ-YFP-mts ring structures externally decorating GUVs (scale bar=10 μm). B) After GUV deflation, inwards conical deformations emerged from FtsZ rings. C) Inspired by deformations in (B), we designed a PDMS microstructure with inwards-conical geometry covered with a supported lipid bilayer (SLB). The imaging plane was chosen to have a cross-section of ~1 μm diameter. D) Inside cones, FtsZ-YFP-mts self-assembled into dynamic vortices (Movie S1). E) Kymograph showed negative and positive slopes indicating the presence of clockwise and anticlockwise directions (Scale bar = 5 μm).

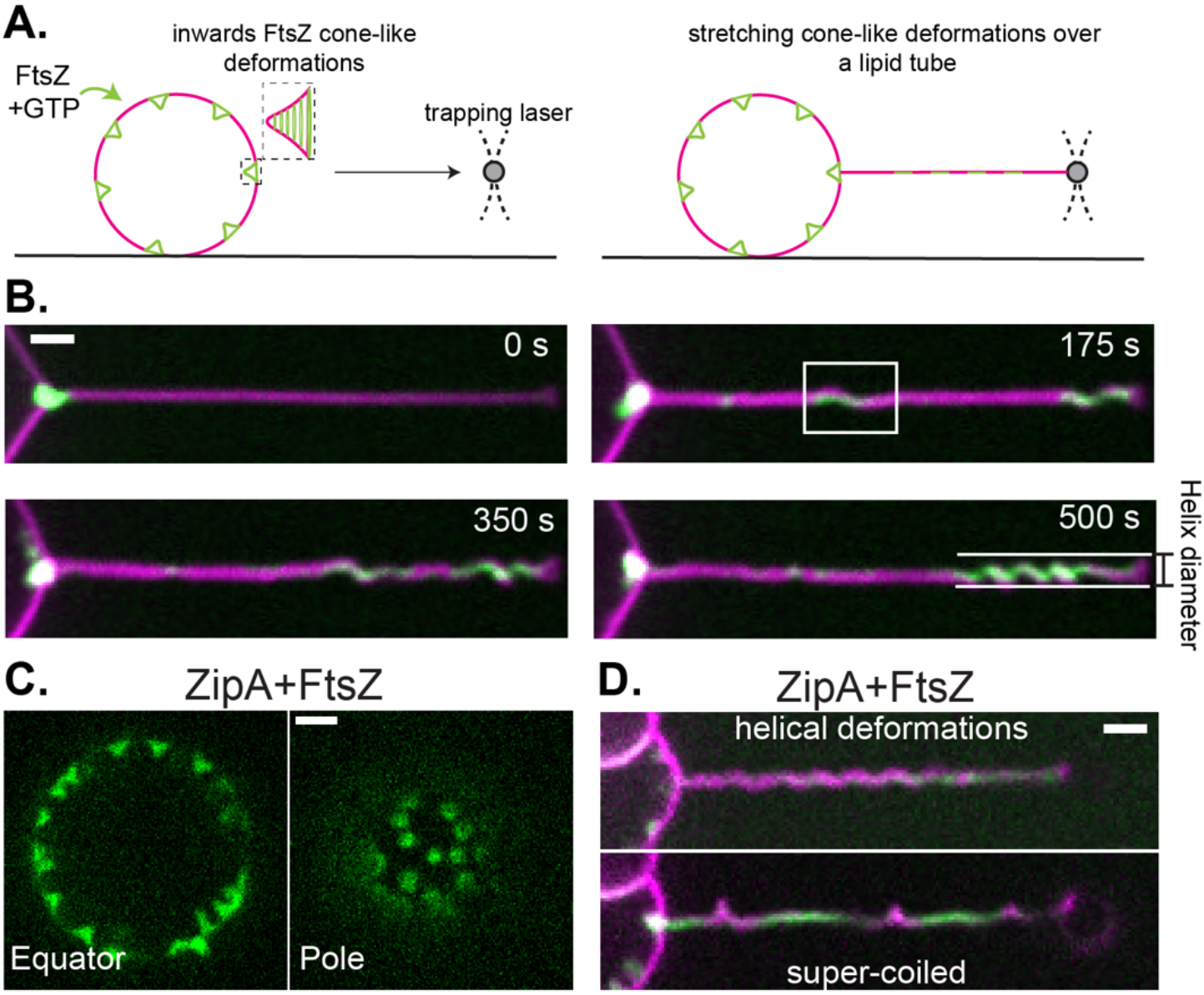

Figure 2

A) To characterize the protein structures forming the cone-like deformations, we stretched the deformed vesicle membrane into a tubular geometry. Large and soft lipid tubes were pulled from weakly surface-attached GUVs by moving the GUVs relative to an optically trapped bead. As soon as the FtsZ-YFP-mts entered the tube, a process of coiling is clearly observed as a function of time. The clustering of protein towards the tip correlate with a spring-like shape. Green and magenta corresponds to fluorescence signal of FtsZ-YFP-mts and lipid respectively. B) To rule out that artificial attachment of the FtsZ-YFP-mts is responsible of the helical transformation, we reconstituted wild-type FtsZ anchored to the membrane via ZipA. When wild type FtsZ was added to ZipA decorated vesicles, rings were self-assembled causing inwards cone-like deformations (N=74) such as in the case of FtsZ-YFP-mts.C) After pulling lipid tubes, similar helical deformations and super coiled regions were observed confirming that torsion is related the

FtsZ core of the polymer (N=3 out of 18 pulled tubes). Fluorescence signal of wt-FtsZ-Alexa 488 is shown in green while siZipA remains unlabeled and lipids are shown in magenta. (Scale bar = 2 μm).

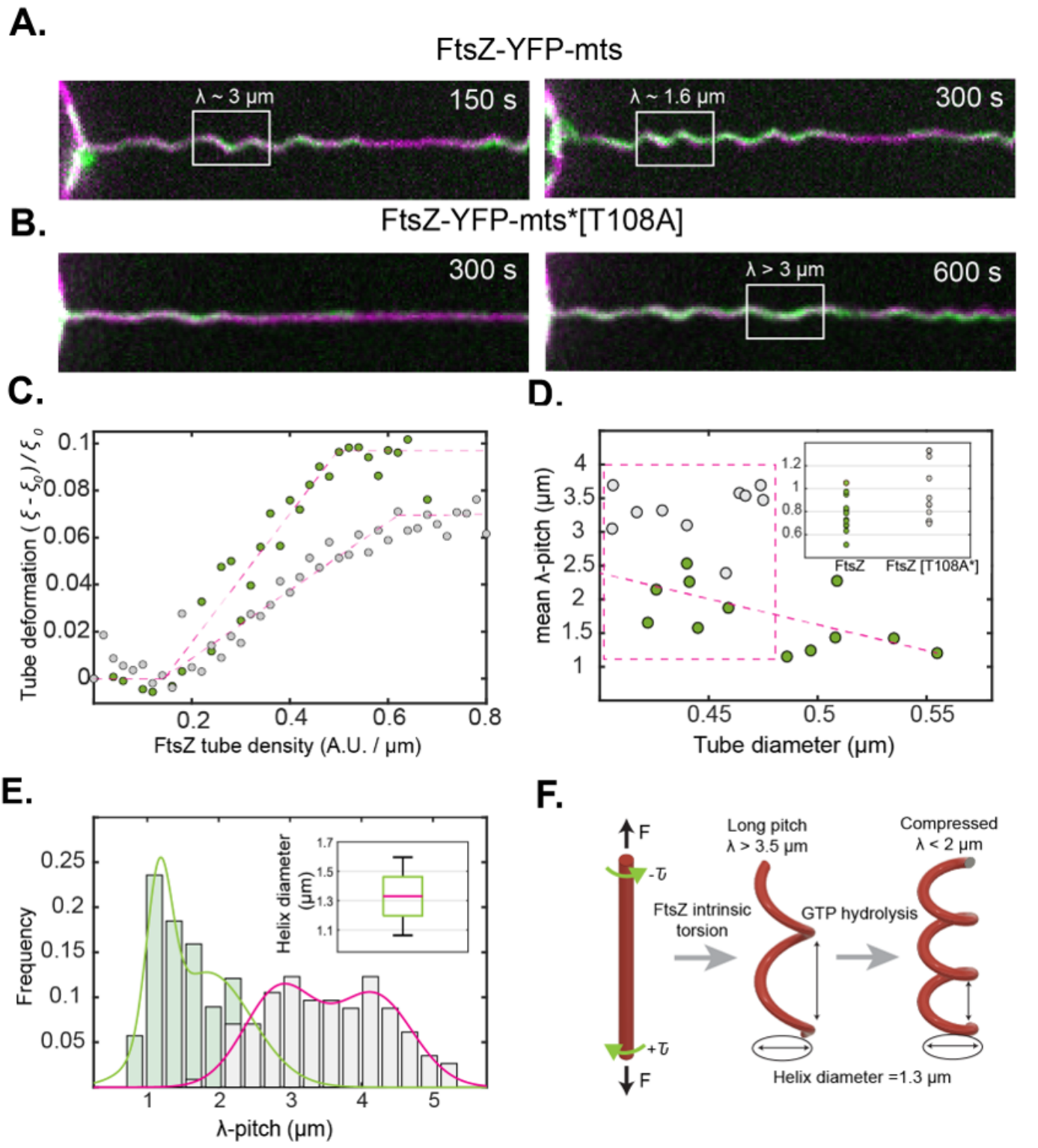

Figure 3

A) FtsZ-YFP-mts and B) FtsZ-YFP-mts*[T108A] promoted helical deformations with the difference that GTPase activity induces compression (λ ~ 1.6 μm) of initially longer pitch (λ > 3 μm). FtsZ-YFP-mts is shown in green while lipids are shown in magenta. C) Tube deformation (arc length) in (A-B) against

FtsZ-YFP-mts (green circles) and FtsZ-YFP-mts*[T108A] (gray circles) tube density, as function of time (Fig. 2SD), evidenced that GTPase activity caused greater tube deformation. D) To rule out that compression was biased by the deflation state, we plotted tube diameter vs mean pitch for FtsZ-YFP-mts (N=12) (green) and FtsZ-YFP-mts*[T108A] (N=10) (gray) in steady state. Despite of higher tube densities for FtsZ-YFP-mts*[T108A] as shown in (D-insert), the mean pitch for no GTPase case is longer at comparable tube diameters. E) We observed two clear pitch states for FtsZ-YFP-mts (light green bars/green line) and FtsZ-YFP-mts*[T108A] (gray bars/magenta line) with a clear dominance of longer pitch for the mutant without GTPase activity. F) Helical deformations can be understood by twisting an elastic rod subjected to constant force. We postulate that FtsZ has an intrinsic torsion that is enhanced by GTPase activity, driving further compression. Intrinsic FtsZ torsion rules long-pitch transformations (λ > 3 μm) while GTP enhances further torsion causing higher pitch states (λ < 2 μm).

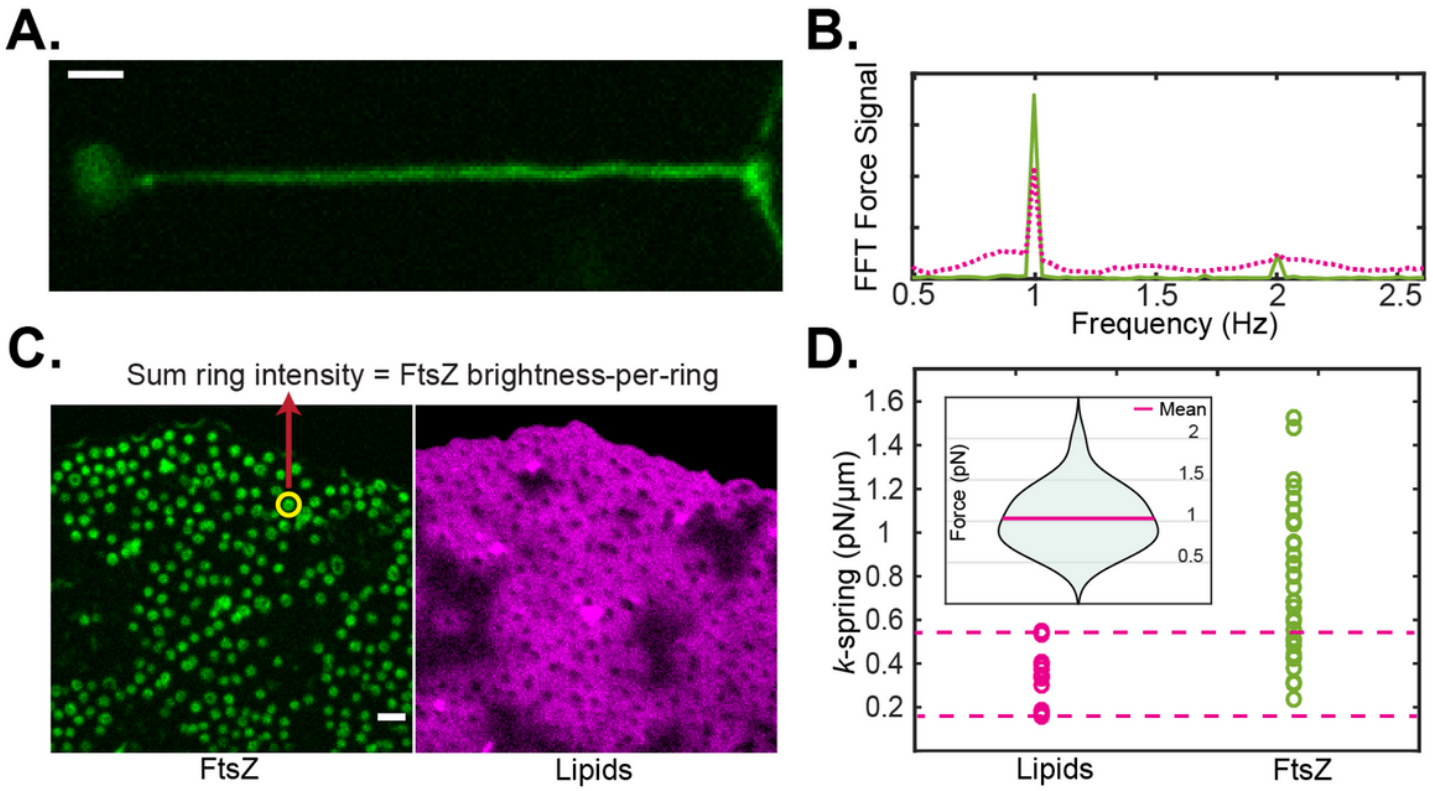

Figure 4

A) Spring-like structures were mechanically assessed by forcing the tube length to oscillate with an amplitude of 3 μm and a frequency of 1Hz. To measure a reliable force contribution from the protein, we increased the protein sample concentration (see M&M) to guarantee a full/high protein coverage of the tube. B) To measure forces, we tracked bead-displacement as response of the dynamic input. Then we Fast Fourier transformed (FFT) the data to calculate the amplitude of the signal. magenta line: lipid signal and green line: FtsZ. C) Spontaneous flattening of vesicles over the glass surface permitted to characterize the total brightness of single rings (N=412) with exactly same conditions as lipid tube experiments. D) By calculating the amplitude of each FFT force signal (B), we assessed the spring constant for the case of the only lipid contribution (N=11) and FtsZ (N=36). Dashed magenta lines

indicate the range where the lipid response dominated over the FtsZ contribution to the spring constant. D-insert) The total FtsZ brightness for each data point in (D) was determined to approximate the FtsZ brightness-per-ring in accordance with Fig. 2SE. Thus, the distribution of forces/ FtsZ brightness-per-ring was plotted (N=23) showing a mean value around 1 pN per ring unit. (Scale bar = 2 μm)

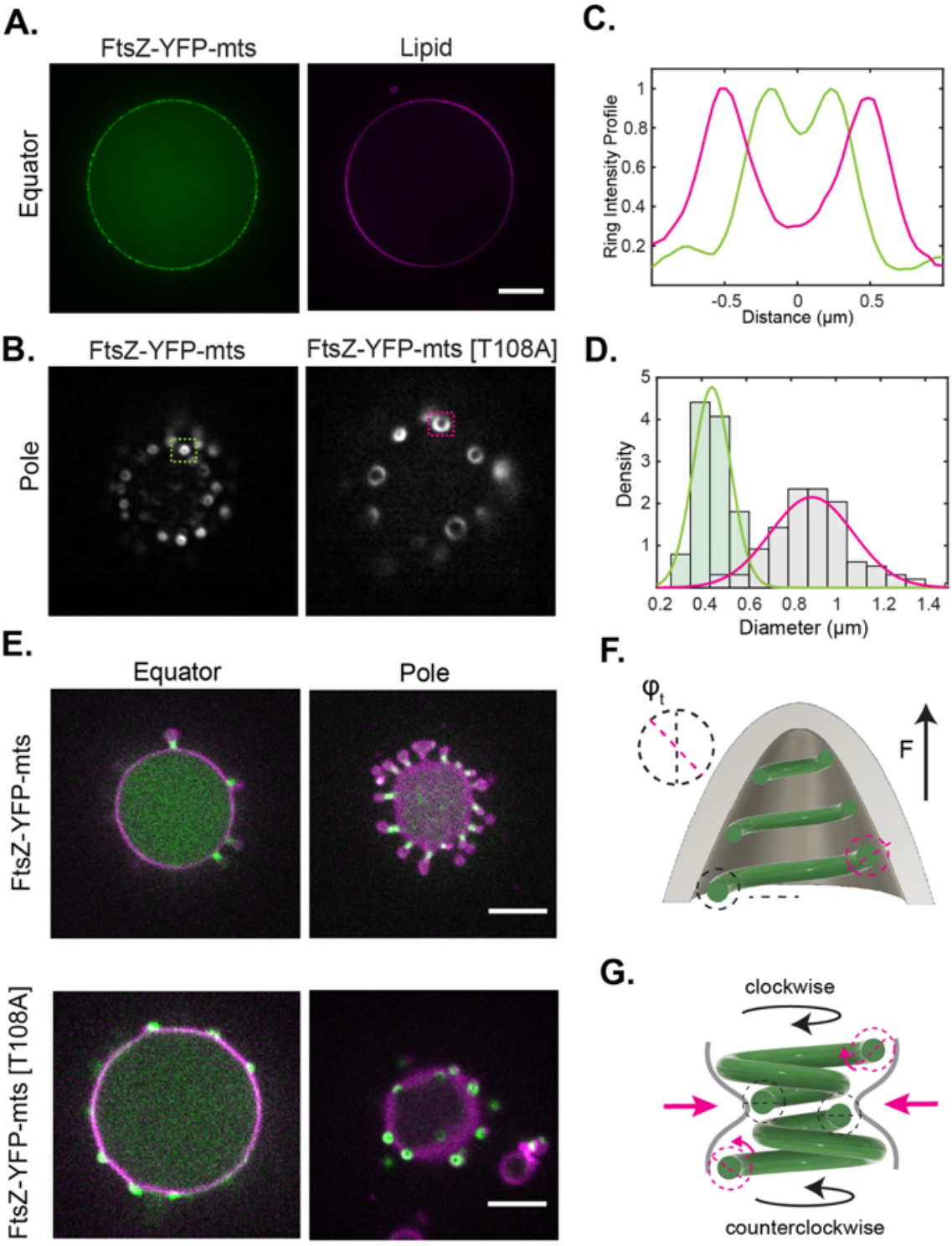

Figure 5

A) FtsZ-YFP-mts and FtsZ-YFP-mts*[T108A] rings inside GUVs. B) Imaging of rings, at GUVs bottom, using TIRF microscopy. C) Intensity profile of structures indicated in (B) showed that FtsZ-YFP-mts (green line) rings exhibit smaller diameter than FtsZ-YFP-mts*[T108A] (magenta line). D) Size distribution of (N=112) FtsZ-YFP-mts*[T108A] (gray bars and magenta line) and (N=102) FtsZ-YFP-mts showed a drastic reduction in ring diameter due to GTP hydrolysis. E) After deflation, both mutants yielded outwards deformations. For the case of FtsZ-YFP-mts, N= 21/26 (80%) vesicles showed outwards deformations and constriction necks compared to N=4/15 (26%) for FtsZ-YFP-mts*[T108A]. This suggests that GTPase activity promotes constriction and neck formation. F) We suggest that intrinsic torsion can create out-of-plane forces; however, G) GTP hydrolysis triggered a super-constricted state favoring higher curvatures. (Scale bar = 5 μm)

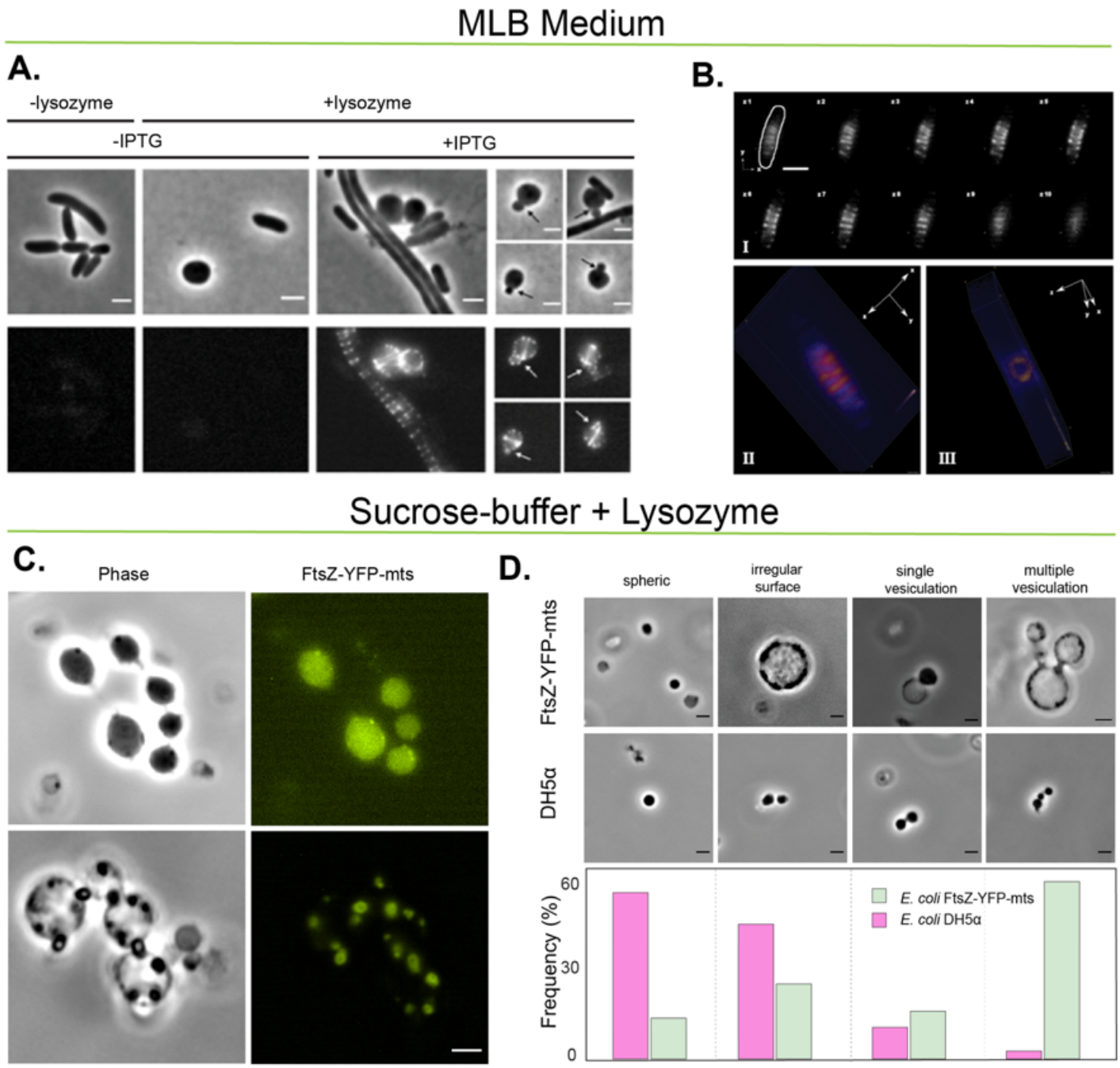

Figure 6

A) E. coli DH5 cells expressing FtsZ-YFP-mts show impaired division and a regular fluorescence pattern. Removal of the cell wall by lysozyme treatment leads to spheroplast formation. Occasional membrane vesiculation can be correlated to the localization of FtsZ-YFP-mts (arrows). B) Upon induction, cells express FtsZ-YFP-mts polymeric structures perpendicular to the cell length, around midcell (BI). 3D rendering reveals ring-like structures (BII-BIII). C) Attempts to enhance the spheroplasting efficiency (sucrose-buffer) resulted in the emergence of multi vesiculated structures. Points of membrane constriction correlate with presence of FtsZ-YFP-mts. Deformations of the plasma membrane indicate a force generation by FtsZ assemblies that leads to local membrane invaginations and eventually pinching off of vesicles. D) Quantitative morphological classification of induced E. coli DH5 pEKEx2-ftsZ-yfp-mts cells (N = 50 cells) compared to E. coli DH5 (N = 43 cells), after lysozyme treatment in sucrose-buffer, within the four categories: spheric, irregular surface, single- and multiple vesiculation. (Scale bar = 2 μm).

Supplementary Files

This is a list of supplementary files associated with this preprint. Click to download.

- MovieS1.mp4
- MovieS2.mp4
- MovieS3.mp4
- MovieS4.mp4
- MovieS5.mp4
- MovieS6.mp4
- SupplementaryTorsionNatCommFinal.docx
- RamirezTorsiondataNatCom.xlsx